Resilient Corner Based Vehicle Velocity Estimation

Mohammad Pirani, Ehsan Hashemi, Amir Khajepour, Baris Fidan, Alireza Kasaiezadeh, Shih-Ken Chen, Bakhtiar Litkouhi

***Abstract*—This paper presents longitudinal and lateral velocity estimators by considering the effect of the suspension compliance at each corner (tire) for ground vehicles. The estimators are developed to be resilient to sensor measurement inaccuracies, model and tire parameter uncertainties, switchings in observer gains, as well as measurement failures. More particularly, the stability of the observer is investigated, and its robustness to road condition uncertainties and sensor noises is analyzed. The sensitivity of the observers' stability and performance to the model parameter changes is discussed. Moreover, the stability of the velocity observers for two cases of arbitrary and stochastic switching gains is investigated. The stochastic stability of the observer in the presence of faulty measurements is also studied, and it is shown that if the probability of a faulty measurement occurring is less than a certain threshold; the observer error dynamics will remain stochastically stable. The performance of the observer and the effect of the suspension compliance are validated via several road experiments.**

***Keywords*—Resilient velocity estimation, Robustness, Switching systems, Vehicle dynamics**

I. Introduction

Vehicle velocity, in both longitudinal and lateral directions, makes major contributions to traction and stability control systems. It can be measured with the advent of GPS; however, the insufficient accuracy of the commonly used conventional GPSs (especially for the lateral direction) and their occasional loss of reception are primary impediments. Two major approaches have been developed in the literature for the estimation of longitudinal and lateral velocities. One is the modified kinematics-based approach, which uses vehicle longitudinal and lateral accelerations and the yaw rate measurements and estimates the vehicle states by employing Kalman Filter based [1] or nonlinear observers [2], [3]. This approach does not employ a tire model, but instead, sensor bias and noise should be identified precisely for a reliable estimation. To remove noises and address the low excitation scenarios, the kinematics-based approach employs accurate GPS data, which imposes additional costs on commercial vehicles.

The other estimation method is model-based and implements tire forces, which requires the road friction and accurate tire parameters. To deal with the varying tire parameters and model uncertainties, a nonlinear observer is provided in [4] with simultaneous bank angle estimation. An Extended Kalman Filter (EKF) is employed for both longitudinal and lateral vehicle state estimation in [5]–[8] to estimate the vehicle states and parameters of the tire model. Similarly, when employing an Unscented Kalman Filter (UKF), [9] estimates the lateral and longitudinal velocities using knowledge of the road condition and the LuGre tire model [10], [11], respectively. A direct virtual sensor moving horizon estimator (MHE) is provided in [12] for estimation of the vehicle side-slip angles with a nonlinear finite impulse response filter.

To address the unknown road friction, other literature focus on state estimation and road identification at the same time [13]. A nonlinear side slip observer is proposed in [14] to identify the road condition and estimate vehicle states simultaneously. In [15], a sliding-mode observer is proposed to estimate velocities using braking torque, longitudinal/lateral acceleration measurements, and an EKF for the estimation of road friction. An adaptive side slip angle estimation based on the Brush tire model and vehicle aligning moment that simultaneously identifies the road condition is proposed by [16]. However, these methods need tire parameters in presence of tire wear, and inflation pressure changes. Moreover, an adaptive vehicle estimation and control [17] in the presence of unknown road friction requires a certain level of excitation which may not be applicable in reality.

Therefore, reliable velocity estimation robust to road uncertainties and model parameter variations has been underlined in recent stability control methods. A coupled kinematic and model-based approach is developed in [18] to estimate longitudinal relative velocities at each corner. In order to design a reliable vehicle velocity estimator, a precise vehicle model is needed. The imprecision of the vehicle dynamics can be rooted in an inaccurate tire model or by omitting additional dynamics, such as the effect of the suspension compliance on the tire kinematics. Hence, in order to reliably design a velocity estimator, an accurate model augmented by the suspension compliance is needed, which is addressed in this article. To accommodate high-slip cases, the observer gains change accordingly and form a switched system. Stability of the velocity observers at each corner are also investigated in this paper. Based on the above discussion, this paper addresses the following issues:

- A corner-based velocity estimation for both longitudinal and lateral directions is developed by considering the effect of the suspension compliance using a coupled kinematic and model-based method. The performance of the estimator is also analyzed.
- The stability of the observer for the general time-varying case and its robustness to road condition uncertainties and sensor noises are discussed. Moreover, sensitivity analysis of the observers' stability and robustness to the model's parameter changes is carried out.

Mohammad Pirani, Ehsan Hashemi, Amir Khajepour and Baris Fidan are with the Department of Mechanical and Mechatronics Engineering, University of Waterloo, ON, Canada, N2L 3G1 email: mpirani, ehashemi, a.khajepour, fidan@uwaterloo.ca

Alireza Kasaiezadeh, Shih-Ken Chen, and Bakhtiar Litkouhi are with the R&D Department, General Motors Co., Warren, MI 48093, USA

- The stability of the velocity observers under gain switching for two cases of arbitrary and stochastic switching and the effect of knowing about the switching policies are studied.
- Stochastic stability of the observer in presence of faulty measurements is also analyzed. This provides a measure for the resilience of the velocity observer to the cascading failure.

The structure of the paper is as follows. The longitudinal and lateral velocity estimators are provided in section II. The suspension compliance effect and its incorporation in the velocity estimators are studied in section III. The stability of the linear parameter-varying error dynamics, the $\mathcal{H}_\infty$ robustness, and sensitivity to tire parameters are investigated in section IV. Stability analysis of the systems under arbitrary and stochastic observer gain switchings and a comparison between the two switching policies are carried out in Section V. Section VI discusses the stochastic stability of the observer in the presence of faulty measurements. Experimental results are presented in section VII to show the performance of the state estimation approach on various road frictions and in maneuvers with longitudinal/lateral excitations. Section VIII presents conclusions.

II. Velocity Estimation at Each Corner

The vehicle velocity observer in this section is a new design of the estimator in [18] which has coupled the kinematics-based (tire-free) approach and the tire's internal states at each corner to estimate relative velocities. The selected tire model is the average lumped LuGre [19] because of the dynamics in the internal deflection state as described in the following subsection. The vehicle and tire parameters (with their actual values used for experiments) are presented in Table (I).

TABLE I: Vehicle Specifications and Tire Parameters/states

Description	Parameter/State	Unit	Value
Rubber stiffness	σ_{0x}, σ_{0y}	$[1/m]$	641, 131.5
Rubber damping	σ_{1x}, σ_{1y}	$[s/m]$	0.85, 0.82
Relative viscous damping	σ_{2x}, σ_{2y}	$[s/m]$	0.0016, 0.001
Load distribution factor	κ_x, κ_y	$[s/m]$	8.1, 13.4
Vehicle mass	m	$[kg]$	2330
Vehicle moment of inertia	I_z	$[kg.m^2]$	4650
Wheel moment of inertia	I_w	$[kg.m^2]$	1.65
Front & rear axles to CG	L_f, L_r	$[m]$	1.42, 1.43
Effective radius	R_e	$[m]$	0.33
Vehicle tire center velocity	V_{xt}, V_{yt}	$[m/s]$	–
Vehicle corner velocity	V_{xc}, V_{yc}	$[m/s]$	–
Tire relative velocity	V_{rx}, V_{ry}	$[m/s]$	–
Wheel speed	ω	$[rad/s]$	–
LuGre friction state	z_x, z_y	$[-]$	–
Long/Lat tire force	F_x, F_y	$[N]$	–
Normalized Coulomb friction	μ_c	$[-]$	0.85
Normalized static friction	μ_s	$[-]$	1.1
Stribeck velocity	V_s	$[m/s]$	5
Vehicle yaw rate	r	$[rad/s]$	–
Vehicle long/lat acceleration	a_x, a_y	$[m/s^2]$	–
Suspension stiffness	K_x, K_y	$[N/m]$	3e5, 7e5
Suspension damping	C_x, C_y	$[Ns/m]$	3730
Quarter car unsprung mass	M_u	$[kg]$	46
Front/Rear track length	T_{rf}, T_{rr}	$[m]$	1.62, 1.56
CG height	h_{CG}	$[m]$	0.65
Front/Rear axles to CG	d_f, d_r	$[m]$	1.42, 1.43
Height of the roll center	h_{RC}	$[m]$	0.54

A. LuGre Tire Model

The internal longitudinal and lateral states z_q ($q \in \{x, y\}$)[1]. and the normalized tire forces f_{nq} (i.e. $f_{nx} = F_x/F_z, f_{ny} = F_y/F_z$) in the pure-slip case are described as follows in the LuGre model:

$$\dot{z}_q = V_{rq} - (\kappa_q R_e|\omega| + \frac{\sigma_{0q}|V_{rq}|}{\theta g(V_{rq})})z_q, \tag{1}$$

$$f_{nq} = \sigma_{0q} z_q + \sigma_{1q}\dot{z}_q + \sigma_{2q} V_{rq}, \tag{2}$$

in which ω is the wheel speed and $V_{rx} = R_e\omega - V_{xt}$, $V_{ry} = -V_{yt}$ are the longitudinal/lateral relative velocities. The tires' center velocities in the tire coordinates are denoted by V_{xt}, V_{yt}. The function, $g(V_{rq})$ in the pure-slip model is defined as $g(V_{rq}) = \mu_c + (\mu_s - \mu_c)e^{-|\frac{V_{rq}}{V_s}|^{0.5}}$. The effect of pure and combined-slip LuGre tire models in the vehicle stability is explored in [20]. The parameter $\theta \in [0, 1]$ in (1) represents the road condition which is small when the road is slippery and it is close to 1 otherwise. In the following subsection, θ is assumed to be unknown which results in unknown term $\frac{\sigma_{0q}|V_{rq}|}{\theta g(V_{rq})} z_q$ in (1).

B. Longitudinal velocity estimation

Assuming the unknown road friction term $\frac{\sigma_{0q}|v_{rq}|}{\theta g(v_{rq})} z_q$ as the bounded uncertainty ϱ_{zx}, one can write the LuGre model (1) as follows at each corner for the longitudinal direction:

$$\dot{z}_x = V_{rx} - \kappa_x R_e|\omega| z_x + \varrho_{zx}. \tag{3}$$

The time derivative of the longitudinal relative velocity is described as:

$$\dot{V}_{rx} = R_e\dot{\omega} - \dot{V}_{xt} + \varrho_{ax}, \tag{4}$$

However the measured signals $\dot{V}_{xt}$ and ω (and particularly its derivative $\dot{\omega}$) are corrupted due to the sensor noises and bias. The deviation of the measured relative acceleration $R_e\dot{\omega} - \dot{V}_{xt}$ from $\dot{V}_{rx}$ at each corner due to the sensor noises is denoted by ϱ_{ax}. The value of the longitudinal acceleration at CG (measured by IMU) is projected into the tires' center $\dot{V}_{xt}$.

Dynamics of the tire internal states (3) together with relative velocities (4) are used to develop the following dynamics:

$$\dot{\mathbf{x}} = \begin{bmatrix} -\kappa_x R_e|\omega| & 1 \\ 0 & 0 \end{bmatrix} \mathbf{x} + \mathbf{B}_x u_x + \boldsymbol{\varrho}_x, \tag{5}$$

in which $\mathbf{B}_x = [0 \quad 1]^T$, uncertainties are denoted by $\boldsymbol{\varrho}_x = [\varrho_{zx} \quad \varrho_{ax}]^T$, the states are $\mathbf{x} = [z_x \quad V_{rx}]^T$, and $u_x = R_e\dot{\omega} - \dot{V}_{xt}$. Substituting $\dot{z}_x$ from (3) into the normalized longitudinal force of the pure-slip case (2), one can rewrite the output equation as:

$$\begin{aligned} f_{nx} &= [(\sigma_{0x} - \sigma_{1x}\kappa_x R_e|\omega|) \quad (\sigma_{1x} + \sigma_{2x})]\mathbf{x} + \sigma_{1x}\varrho_{zx} \\ &= \mathbf{C}_x(\omega)\mathbf{x} + \sigma_{1x}\varrho_{zx}. \end{aligned} \tag{6}$$

[1]From now, an index q for tire states or parameters indicates the direction of interest, i.e. $q \in \{x, y\}$. Tire forces and velocities in tire coordinates are shown in Fig. 1 (b).

By employing the normalized longitudinal force (6) and the system (5), the following observer is obtained for longitudinal velocity estimation with the estimated output $\hat{y} = \hat{f}_{nx} = \mathbf{C}_x(\omega)\hat{\mathbf{x}}$ and observer gains $\mathbf{L}_x = [L_{1x} \quad L_{2x}]^T$:

$$\dot{\hat{\mathbf{x}}} = \mathbf{A}_x(\omega)\hat{\mathbf{x}} + \mathbf{B}_x u_x + \mathbf{L}_x(f_{nx} - \hat{f}_{nx}), \tag{7}$$

where $f_{nx} = F_x/F_z$ is the normalized longitudinal tire force. The bounded time-varying parameter in (7) is the wheel speed and the parameter varying state transition matrix is $\mathbf{A}_x(\omega) \in \mathbb{R}^{2\times 2}$. The error dynamics $\mathbf{e}_x = \mathbf{x} - \hat{\mathbf{x}}$ from (5) and (7) yields:

$$\begin{aligned}\dot{\mathbf{e}}_x &= [\mathbf{A}_x(\omega) - \mathbf{L}_x\mathbf{C}_x]\mathbf{e}_x - \mathbf{L}_x\sigma_{1x}\varrho_{zx} + \boldsymbol{\varrho}_x \\ &= \mathbf{A}_{e_x}(\omega)\mathbf{e}_x + \begin{bmatrix} 1 - L_{1x}\sigma_{1x} & 0 \\ -L_{2x}\sigma_{1x} & 1 \end{bmatrix} \boldsymbol{\varrho}_x \\ &= \mathbf{A}_{e_x}(\omega)\mathbf{e}_x + \mathbf{B}_{e_x}\boldsymbol{\varrho}_x. \end{aligned} \tag{8}$$

The system matrix $\mathbf{A}_x(\omega)$ in (7) is physically bounded; thus, a conventional observability test is performed. The observability matrix for parameter-varying systems like (5) with output (6) is given by [21] as:

$$\begin{aligned} \mathcal{O}_n &= [\epsilon_1 \quad \epsilon_2 ... \quad \epsilon_n]^T, \\ \epsilon_1 = \mathbf{C}_x, &\quad \epsilon_{i+1} = \epsilon_i \mathbf{A}_x(\omega) + \dot{\epsilon}_i. \end{aligned} \tag{9}$$

Observability is confirmed by holding the full rank condition $rank(\mathcal{O}_2) = 2$ at each fixed time span for the operating regions of the wheel speed and its time derivatives. Thus, the parameter-varying system (5) with output (6) is observable, and it is feasible to estimate the longitudinal tire internal states $\hat{z}_x$ and the relative velocity $\hat{V}_{rx}$ by employing the longitudinal force as the output.

Remark 1: For implementation and the road experiments, discretization of the continuous-time system (5) with the output $y = \mathbf{C}_x\mathbf{x} + \mathbf{D}_x u_x$ is done by the Step-Invariance method because of its precision and response characteristics. The step-invariance discretization is the zero-order hold method and includes constant input signal $u_x(t)$ during integration. It has good accuracy with the platform sampling frequency of $200[Hz]$. Moreover the richness of the step signal, in terms of the frequencies that it carries, makes the step invariance method very suitable for automotive applications, as there exist a large amount of uncertainties and disturbances. Input to the continuous-time system is the hold signal $u_x[k] = u_x[t_k]$ for a period between $t_k \leq t < t_{k+1}$ with the sample time T_s. Then, the discrete-time system $\mathbf{x}[k+1] = \mathbf{A}_x^d[k]\mathbf{x}[k] + \mathbf{B}_x^d u_x[k], y[k] = \mathbf{C}_x^d\mathbf{x}[k] + \mathbf{D}_x^d u_x[k]$ has the output matrices $\mathbf{C}_x^d = \mathbf{C}_x, \mathbf{D}_x^d = \mathbf{D}_x$ and state/input matrices:

$$\mathbf{A}_x^d = e^{\mathbf{A}_x(t)T_s}, \quad \mathbf{B}_x^d = \int_0^{T_s} e^{\mathbf{A}_x(t)\tau}\mathbf{B}_x(t)d\tau. \tag{10}$$

The discretized from of the error dynamics (8), can now be written as $\mathbf{e}_x[k+1] = \mathbf{A}_{e_x}^d[k]\mathbf{e}_x[k] + \mathbf{B}_{e_x}^d\boldsymbol{\varrho}_x[k]$. The following subsection focuses on the corner-based velocity observer for the lateral direction. □

C. Lateral velocity estimation

The LuGre output equation (2) for the lateral direction can be expressed as follows:

$$\begin{aligned} f_{ny} &= [(\sigma_{0y} - \sigma_{1y}\kappa_y R_e|\omega|) \quad (\sigma_{1y} + \sigma_{2y})]\bar{\mathbf{x}} + \sigma_{1y}\varrho_{zy} \\ &= \mathbf{C}_y(\omega)\bar{\mathbf{x}} + \sigma_{1y}\varrho_{zy}, \end{aligned} \tag{11}$$

where the states are $\bar{\mathbf{x}} = [z_y \quad V_{ry}]^T$. The relative lateral acceleration $\dot{V}_{ry} = -\dot{V}_{yt} + \varrho_{ay}$ (the projected lateral acceleration in the tire coordinate system is denoted by $\dot{V}_{yt}$) is combined with the lateral LuGre internal state to form the lateral velocity estimator. Equation (5) can be rewritten for the lateral direction as $\dot{\bar{\mathbf{x}}} = \mathbf{A}_y(\omega)\bar{\mathbf{x}} + \mathbf{B}_y u_y + \boldsymbol{\varrho}_y$ using state and input matrices $\mathbf{A}_y = [-\kappa_y R_e|\omega| \quad 1; 0 \quad 0], \mathbf{B}_y = \mathbf{B}_x$, and $u_y = -\dot{v}_{yt}$. Uncertainties in the lateral states are denoted by $\boldsymbol{\varrho}_y = [\varrho_{zy} \quad \varrho_{ay}]^T$. The state estimator can be expressed as follows for the lateral direction with the output $\hat{y}_l = \hat{f}_{ny} = \mathbf{C}_y(\omega)\hat{\mathbf{x}}_l$:

$$\dot{\hat{\bar{\mathbf{x}}}} = \mathbf{A}_y(\omega)\hat{\bar{\mathbf{x}}} + \mathbf{B}_y u_y + \mathbf{L}_y(f_{ny} - \hat{f}_{ny}), \tag{12}$$

in which $\mathbf{L}_y = [L_{1y} \quad L_{2y}]^T$.

Remark 2: Similar to the longitudinal direction, the observability of the lateral direction dynamics can be verified by the observability criterion (9) for the parameter-varying system with $\mathbf{A}_y(\omega), \mathbf{C}_y(\omega)$. □

The error dynamics is then derived as follows for the lateral velocity estimator and represents a linear parameter varying system:

$$\dot{\mathbf{e}}_y = \mathbf{A}_{e_y}(\omega)\mathbf{e}_y + \underbrace{\begin{bmatrix} 1 - L_{1y}\sigma_{1y} & 0 \\ -L_{2y}\sigma_{1y} & 1 \end{bmatrix}}_{\mathbf{B}_{e_y}} \boldsymbol{\varrho}_y, \tag{13}$$

where $\mathbf{A}_{e_y} = [\mathbf{A}_y(\omega) - \mathbf{L}_y\mathbf{C}_y]$. The error dynamics in discrete-time yields $\mathbf{e}_y[k+1] = \mathbf{A}_{e_y}^d[k]\mathbf{e}_y[k] + \mathbf{B}_{e_y}^d\boldsymbol{\varrho}_y[k]$. In order to increase the accuracy of the velocity estimation at each corner, the effect of the suspension compliance is considered on the estimators and is discussed in the following section.

III. Velocity Estimation with Suspension Compliance

The corner based velocity estimators presented in the previous section are based on the coordinate attached to the vehicle chassis. However, there exists an extra degree of freedom between the chassis and the tire due to the suspension compliance, which should be taken into account. In this section, the effect of the suspension compliance in the modification of the estimated velocities provided in section II is discussed. The dynamics can be represented by a second-order system as $M_u\ddot{\psi}_q(t) + C_q\dot{\psi}_q(t) + K_q\psi_q(t) = F_q$. The displacements due to the suspension in each direction are denoted by $\psi_q(t)$. The suspension dynamics at each corner can be written in the following state space form:

$$\begin{bmatrix} \dot{\psi}_q(t) \\ \ddot{\psi}_q(t) \end{bmatrix} = \begin{bmatrix} 0 & 1 \\ \frac{-K_q}{M_u} & \frac{-C_q}{M_u} \end{bmatrix} \begin{bmatrix} \psi_q(t) \\ \dot{\psi}_q(t) \end{bmatrix} + \begin{bmatrix} 0 \\ 1 \end{bmatrix} \frac{F_q}{M_u}. \tag{14}$$

The velocity term $\dot{\psi}_q(t)$ should be directly added to the estimated velocity at each corner due to the dynamics (14). Thus, the objective is to find the state $\dot{\psi}_q(t)$ in (14) for implementation in the velocity estimation at each corner.

The estimated relative velocities $\hat{V}_{rx}$ and $\hat{V}_{ry}$ by (7), (12) are used for the longitudinal velocity estimation at the tire coordinates as $\hat{V}_{xt} = R_e\omega - \hat{V}_{rx}$ and $\hat{V}_{yt} = -\hat{V}_{ry}$. Afterwards, utilizing the steering angle δ at the front and rear tracks (i.e. $\delta = 0$ for the rear track of front-steering vehicles), each corner's velocity in the vehicle coordinates yields $\hat{\bar{V}}_{xc} = \hat{V}_{xt}\cos\delta - \hat{V}_{yt}\sin\delta$ for the longitudinal direction and $\hat{\bar{V}}_{yc} = \hat{V}_{xt}\sin\delta + \hat{V}_{yt}\cos\delta$ for the lateral direction. The velocities due to the suspension compliance (14) is then added to the estimated velocities in the vehicle coordinates as:

$$\hat{V}_{xc} = \hat{\bar{V}}_{xc} + \dot{\psi}_x, \quad \hat{V}_{yc} = \hat{\bar{V}}_{yc} + \dot{\psi}_y. \tag{15}$$

Estimated corner velocities (15) are then used for calculation of the vehicle's velocity at CG. The longitudinal velocity of the vehicle at its CG, $\hat{V}_x$, is calculated by the front axle speed $\hat{V}_x = 0.5(\hat{V}_{xc_{fL}} + \hat{V}_{xc_{fR}})$ or the rear axle speed $\hat{V}_x = 0.5(\hat{V}_{xc_{rL}} + \hat{V}_{xc_{rR}})$ where fL, fR, rL, rR represent the front-left, front-right, rear-left, and rear-right tires, respectively.

The lateral velocity at the vehicle's CG, $\hat{V}_y$, can be calculated from the front axle's lateral speed $\hat{V}_y = -rL_f + 0.5(\hat{V}_{y_{fL}} + \hat{V}_{y_{fR}})$ or the rear axle's lateral speed $\hat{V}_y = rL_r + 0.5(\hat{V}_{y_{rL}} + \hat{V}_{y_{rR}})$ in which r is the yaw rate and L_f and L_r are the distances from the front and rear axles to CG.

In order to check the performance of the estimators with the suspension compliance, the relative velocities (i.e. slip ratio/angle) corrected by the suspension dynamics are employed in a tire model to calculate the tire forces. The calculated tire forces are then compared to the measured ones to determine Δf_n, which represents the difference between the measured and estimated tire forces with (and without) consideration of the suspension compliance. The experimental validation of this approach is discussed in Section VII. It will be shown in the experimental results that the effect of the suspension compliance is during harsh traction and braking maneuvers where the applied tire forces are considerable. Such effect in a tiny time interval plays an important role in detecting tire slip more accurately and consequently on vehicle traction and stability control.

The structure of the augmented velocity estimators with the Suspension Compliance (SC) effect is depicted in Fig. 1. Considering road friction and measurement noises as uncertainties, the kinematics-based velocity estimation is combined with the internal tire states in *Long. Velocity Est.* and *Lat. Velocity Est.* Measured accelerations by the IMU attached to the sprung mass are corrected with the vehicle's body pitch and roll angles to include only the kinematics of the motion. These corrected values are then used in the velocity estimators. A high-slip detection algorithm is used for appropriate observer gain switch to tackle the slippery cases. Estimated corner velocities are augmented with the suspension effect and mapped onto the vehicle's CG in the *SC and Mapping* module.

Remark 3: Tire forces can be measured by wheel sensors. However, because of high cost impact on production vehicles, installation problems, and maintenance issues, tire force estimation has extensively been tried in the literature. Longitudinal and lateral tire forces at each corner can be estimated using nonlinear and sliding mode observers [22], [23], unknown input observers [24], [25], or Kalman Filter based estimators [26]–[28]. Normalized longitudinal and lateral forces f_{nx}, f_{ny} are assumed to be known from the Kalman Filter based estimation on wheel and lateral dynamics [28], [29]. Due to the fact that the vehicle normal force has a significant impact on normalized longitudinal and lateral tire forces, a detailed study on tire normal force calculation is done in [29]. The detailed procedure of normal force calculation is discussed in Section VII. Since tire forces are used as measurements for the velocity estimation in this paper, they are referred to as *force measurement* and *force estimation* interchangeably. □

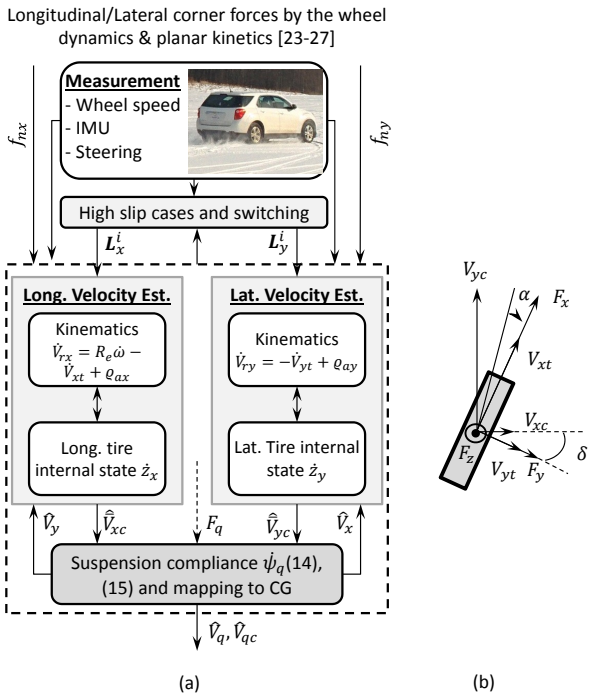

Fig. 1: (a) State estimation structure with SC, (b) Forces and velocities in the tire coordinates.

IV. Estimator's Stability, Robustness and Sensitivity Analysis

In this section, the stability of the observer error dynamics (8) and (13) is analyzed as a linear time varying system. Moreover, the robustness of the observer dynamics to model uncertainties will be investigated and the sensitivity of the stability margin and $\mathcal{H}_\infty$ robustness to tire parameter variations will be discussed.

A conventional approach is to study the stability of the symmetric part of the matrix, which usually results in conservative results [30]. In order to tackle the conservativeness

issue, a similarity transformation is utilized in the following proposition to show the boundedness of the estimation error.

Proposition 1: Estimation errors in linear time varying error dynamics (8) and (13) are bounded.

Proof: A similarity transformation in the form of $\bar{\mathbf{e}}_q(t) = \mathbf{T}\mathbf{e}_q(t)$ is employed on the longitudinal/lateral estimation error states (8) and (13), which results in $\bar{\mathbf{A}}_{e_q} = \mathbf{T}\mathbf{A}_{e_q}\mathbf{T}^{-1}$ and $\bar{\mathbf{B}}_{e_q} = \mathbf{T}\mathbf{B}_{e_q}$. Choosing $\mathbf{T} = diag(\gamma, 1)$ with a design parameter $\gamma > 0$, leads to $\bar{\mathbf{A}}_{e_q}$ whose stability margin, $\mathcal{SM}_q \triangleq \max_i \lambda_i(\bar{\mathbf{A}}_{e_q})$, is close to the stability margin of its symmetric part (which will be discussed in Example 1 later). Moreover, due to the fact that $||\mathbf{T}||$ and $||\mathbf{T}^{-1}||$ are bounded, the transformation matrix $\mathbf{T}$ preserves the exponential stability and the exponent (rate) of the convergence [31], [32]. The Lyapunov candidate $\mathcal{V}(\bar{\mathbf{e}}_q(t)) = \frac{1}{2}\bar{\mathbf{e}}_q(t)^T\bar{\mathbf{e}}_q(t)$ is then introduced to investigate the stability of the error dynamics (8) and (13)[2]. The time derivative of the Lyapunov function along the state trajectories leads to

$$
\begin{aligned}
\dot{\mathcal{V}} &= \frac{1}{2}\dot{\bar{\mathbf{e}}}_q(t)^T\bar{\mathbf{e}}_q(t) + \frac{1}{2}\bar{\mathbf{e}}_q^T(t)\dot{\bar{\mathbf{e}}}_q(t), \\
&= \bar{\mathbf{e}}_q^T(t)\underbrace{\left(\frac{1}{2}\left(\bar{\mathbf{A}}_{e_q}^T + \bar{\mathbf{A}}_{e_q}\right)\right)}_{\bar{\mathbf{A}}_s}\bar{\mathbf{e}}_q(t) \\
&+ \frac{1}{2}\left(\boldsymbol{\varrho}_q^T\bar{\mathbf{B}}_{e_q}^T\bar{\mathbf{e}}_q(t) + \bar{\mathbf{e}}_q^T(t)\bar{\mathbf{B}}_{e_q}\boldsymbol{\varrho}_q\right) \\
&\leq \lambda_{\max}(\bar{\mathbf{A}}_s)||\bar{\mathbf{e}}_q(t)||^2 + \frac{1}{2}\left(\frac{1}{2\epsilon}\boldsymbol{\varrho}_q^T\bar{\mathbf{B}}_{e_q}^T\bar{\mathbf{B}}_{e_q}\boldsymbol{\varrho}_q + \frac{\epsilon}{2}||\bar{\mathbf{e}}_q(t)||^2\right) \\
&\leq \left(\lambda_{\max}(\bar{\mathbf{A}}_s) + \frac{\epsilon}{4}\right)||\bar{\mathbf{e}}_q(t)||^2 + \lambda_{\max}(\bar{\mathbf{B}}_{e_q}^T\bar{\mathbf{B}}_{e_q})||\boldsymbol{\varrho}_q||^2 \\
&= 2\left(\lambda_{\max}(\bar{\mathbf{A}}_s) + \frac{\epsilon}{4}\right)\mathcal{V} + \lambda_{\max}(\bar{\mathbf{B}}_{e_q}^T\bar{\mathbf{B}}_{e_q})||\boldsymbol{\varrho}_q||^2 \\
&\leq \eta_1\mathcal{V} + \eta_2, \qquad (16)
\end{aligned}
$$

for some $\eta_1 < 0$ and $\eta_2 > 0$. Here ϵ is chosen such that $0 < \epsilon \ll |\lambda_{\max}(\bar{\mathbf{A}}_s)|$ to have $\lambda_{\max}(\bar{\mathbf{A}}_s) + \frac{\epsilon}{4} < 0$; thus, $\eta_1 < 0$. The fourth line is due to Young's inequality and the fifth line is due to the fact that $\bar{\mathbf{B}}_{e_q}^T\bar{\mathbf{B}}_{e_q}$ is a symmetric matrix. Introducing $\mathcal{U}(\bar{\mathbf{e}}_q(t)) = \mathcal{V}(\bar{\mathbf{e}}_q(t)) + \frac{\eta_2}{\eta_1}$, based on (16) and the Bellman-Gronwall lemma [33], we have $\mathcal{U}(\bar{\mathbf{e}}_q(t)) \leq e^{\eta_1 t}\mathcal{U}(\bar{\mathbf{e}}_q(0))$, which yields:

$$
0 \leq \mathcal{V}(\bar{\mathbf{e}}_q(t)) \leq e^{\eta_1 t}\left(\mathcal{V}(\bar{\mathbf{e}}_q(0)) + \frac{\eta_2}{\eta_1}\right) - \frac{\eta_2}{\eta_1}, \qquad (17)
$$

which results in;

$$
0 \leq ||\bar{\mathbf{e}}_q(t)||^2 \leq e^{\eta_1 t}\left(||\bar{\mathbf{e}}_q(0)||^2 + \frac{2\eta_2}{\eta_1}\right) - \frac{2\eta_2}{\eta_1}. \qquad (18)
$$

$\frac{\eta_2}{\eta_1} < 0$ proves the exponential stability of the nominal part of the error dynamics (8) and (13) (without term $\boldsymbol{\varrho}_q$) and the boundedness of the estimation error $\mathbf{e}_q(t)$. ■

As mentioned in Proposition 1, the transformation matrix $\mathbf{T}$ yields a less conservative stability condition for the symmetric part of $\bar{\mathbf{A}}_{e_q}$ compared to the symmetric part of $\mathbf{A}_{e_q}$. The following example confirms this claim.

Example 1: Consider error dynamics (8) with the observer gains $\mathbf{L}_x = [1.18, \quad 387]^T$. For a particular angular velocity, e.g. $\omega = 40$, the largest eigenvalue of matrix $\mathbf{A}_{e_x}$ and its symmetric parts are $\lambda_{\max}(\mathbf{A}_{ex}) = -327.1$ and $\lambda_{\max}(0.5(\mathbf{A}_{ex} + \mathbf{A}_{ex}^T)) = 108750$, respectively. Thus, the symmetric part is unstable while matrix $\mathbf{A}_{e_x}$ is Hurwitz. However if we use the similarity transformation mentioned in Proposition 1 with $\mathbf{T} = diag(9000, 1)$, the largest eigenvalue of the symmetric part of $\bar{\mathbf{A}}_{e_x}$ is $\lambda_{\max}(\bar{\mathbf{A}}_s) = -326.8$, which is very close to $\lambda_{max}(\bar{\mathbf{A}}_{e_x})$. This shows how much the stability of the symmetric part of a matrix can be conservative and how much an appropriate choice of a similarity transformation can help in overcoming this conservativeness. □

Proposition 1 shows the boundedness of the estimation errors. However, in order to come up with tighter bounds, system $\mathcal{H}_\infty$ norms, defined as $\mathcal{H}_\infty \triangleq \sup_{\omega\in\mathbb{R}} ||\mathbf{G}(j\omega)||_\infty$, for both longitudinal and lateral error dynamics are shown in Figure 2.

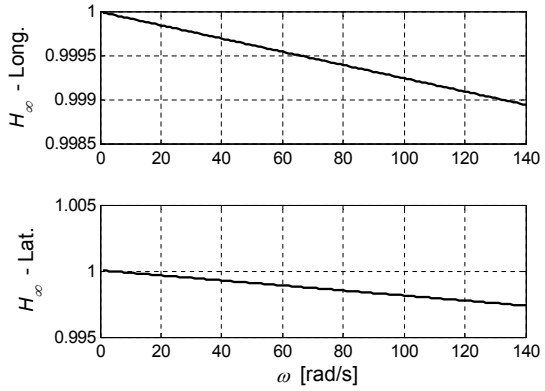

Fig. 2: System $\mathcal{H}_\infty$ norm for longitudinal and lateral estimators

It should be noted that the $\mathcal{H}_\infty$ norm is a conservative system norm and Fig. 2 reveals that even conservative $\mathcal{H}_\infty$ norms of error dynamics are non-expansive ($\mathcal{H}_\infty \leq 1$) for the suggested observers.

Lastly, the sensitivity of the error dynamics stability margin $\mathcal{SM}_q$ and system $\mathcal{H}_\infty$ norms to model parameter uncertainties is investigated. Figs. 3 and 4 show deviation of the stability margin of the error dynamics (8) and (13) from their nominal values due to model parameter deviation of up to 20%.[3] Fig. 5 shows the sensitivity of the system $\mathcal{H}_\infty$ norm of the error dynamics to the same parameter variations. This figure shows that the performance of the observer is not very sensitive to the tire parameter variations.

V. Stability of the Estimator under Gain Switching

To address the high-slip condition, observer gains are switched to change the level of reliance on the output (longi-

[2] $\mathcal{V}(\bar{\mathbf{e}}_q(t))$ and $\mathcal{V}$ are used interchangeably.

[3] Each model parameter $\mathcal{X}$ is perturbed as $\mathcal{X} \pm 0.2\mathcal{X}$.

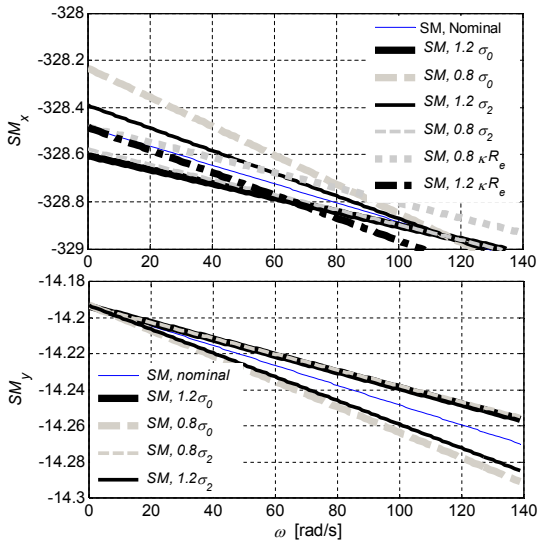

Fig. 3: Sensitivity of $\mathcal{SM}$ of (8) and (13).

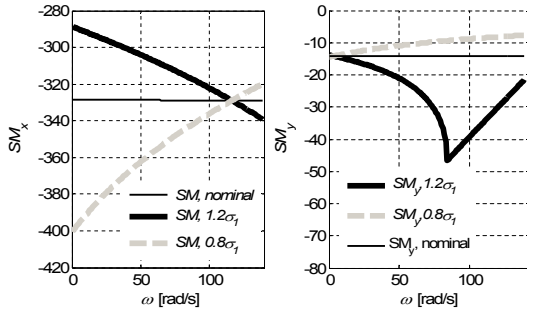

Fig. 4: Sensitivity of $\mathcal{SM}$ of (8) and (13) to σ_{1q}.

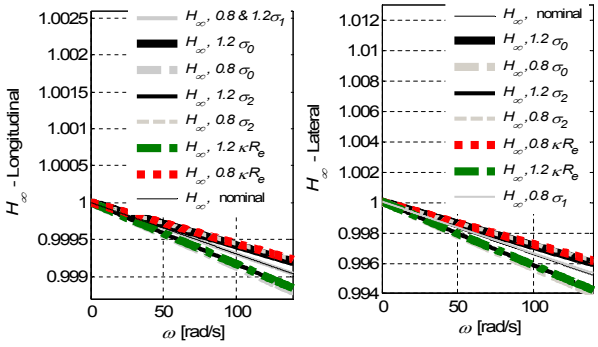

Fig. 5: Sensitivity of $\mathcal{H}_\infty$ norm of (8) and (13).

tudinal/lateral forces and their uncertainties) and process (road friction uncertainties and acceleration noises). The stability of the switched systems has been analyzed extensively under arbitrary [34], [35] and stochastic switching [36]. Switched observers are used in vehicle state or parameter estimation [37].

In this section, the stability of the nominal parts of error dynamics, in the form of (19), is analyzed when the observer gains switch between different modes. In this case, the longitudinal and lateral observer gains can attain each of the two modes to result in:

$$\dot{\mathbf{e}}_q = \mathbf{A}^i_{e_q}(\omega)\mathbf{e}_q, \tag{19}$$

where $\mathbf{A}^i_{e_q}$ belongs to the i-th set of observer gains $\mathbf{L}^i_q$, and $i = 1, 2$ represents switching modes. Since the stability of (19) is a necessary condition for the stability of (8) and (13), it is analyzed in the presence of arbitrary gain switching.

A. Stability of the observer under arbitrarily switching gains

A sufficient condition for the quadratic stability of a switched linear system under arbitrary switching is to have a common quadratic Lyapunov function for all switching modes [34]. Similar to the analysis done in Proposition 1, we introduce the transformed matrix $\bar{\mathbf{A}}^i_{e_q} = \mathbf{T}\mathbf{A}^i_{e_q}\mathbf{T}^{-1}$ with the same transformation matrix $\mathbf{T}$ used in Proposition 1. By choosing the Lyapunov function $\mathcal{V}(\bar{\mathbf{e}}_q) = \frac{1}{2}\bar{\mathbf{e}}_q^T\bar{\mathbf{e}}_q$, one can write:

$$\begin{aligned}\dot{\mathcal{V}} &= \frac{1}{2}\dot{\bar{\mathbf{e}}}_q(t)^T\bar{\mathbf{e}}_q + \frac{1}{2}\bar{\mathbf{e}}_q^T(t)\dot{\bar{\mathbf{e}}}_q(t)\\ &= \bar{\mathbf{e}}_q^T(t)\underbrace{\left(\frac{1}{2}\left(\bar{\mathbf{A}}^{i^T}_{e_q} + \bar{\mathbf{A}}^i_{e_q}\right)\right)}_{\bar{\mathbf{A}}^i_s}\bar{\mathbf{e}}_q \le \lambda_{\max}(\bar{\mathbf{A}}^i_s)||\bar{\mathbf{e}}_q||^2\\ &= 2\lambda_{\max}(\bar{\mathbf{A}}^i_s)\mathcal{V} \le \bar{\lambda}\mathcal{V},\end{aligned} \tag{20}$$

where $\bar{\lambda} = \max_{i=1,2}\{\max_{t\ge 0}\{2\lambda_{max}(\bar{\mathbf{A}}^i_s)\}\}$. This shows that the decaying rate of the switched system is based on the worst case decaying rate over time and over switching modes. This is due to the lack of knowledge about the switching policy. In the following subsection, the stability of the suggested observers under stochastic gain switching is analyzed, and the results will be compared with the case of arbitrary switching.

B. Stability of the observer under stochastically switching gains

In this subsection, switching between the observer gains is assumed to happen in the form of a particular stochastic process represented by a Markov chain. The stability of the Markov jump linear systems has been analyzed vastly [36], [38], [39]. Similar to the arbitrary switching case mentioned in the previous section, stochastic switching will introduce a dynamics that comprises of two sub-dynamics [4]. The switching mechanism is modeled using a Markov chain with the probability transition matrix:

$$\mathbf{P} = \begin{bmatrix} p_{11} & p_{12} \\ p_{21} & p_{22} \end{bmatrix}, \tag{21}$$

[4]Since the switching forms a Markov jump linear system and theoretical results (e.g. Theorem 1) for such systems are derived for discrete time case, the discrete version of the estimator with the sampling time $T = 5$ms is used in the experiment setup.

where $p_{ij} = \mathbf{Pr}(\mathcal{L}[k+1] = \mathbf{L}_q^j | \mathcal{L}[k] = \mathbf{L}_q^i)$. Here, $\mathcal{L}$ is a random vector that takes its values from the sample space $\mathcal{S} = \{\mathbf{L}_q^1, \mathbf{L}_q^2\}$, which are the two sets of observer gains. The following definition is required to investigate the stability of such switched system.

Definition 1 ([40]): The linear system $\mathbf{e}_q[k+1] = \mathbf{A}_{e_q}^{d_i}\mathbf{e}_q[k]$ (matrix $\mathbf{A}_{e_q}^{d_i}$ is the discrete version of $\mathbf{A}_{e_q}^{i}$ in the error dynamics (19), as discussed in Remark 1) is called mean square stable (MSS) if $\lim_{k\to\infty}\mathbb{E}(\mathbf{e}_q[k]^T\mathbf{e}_q[k]) = 0$. □

Based on Definition 1, the following theorem is used for the mean square stability of the error dynamics.

Theorem 1 ([41]): The linear system $\mathbf{e}_q[k+1] = \mathbf{A}_{e_q}^{d_i}\mathbf{e}_q[k]$ is MSS if and only if the following condition holds.

$$\rho\left[(\mathbf{P}^T \otimes \mathbf{I})diag(\mathbf{A}_{e_q}^{d_i} \otimes \mathbf{A}_{e_q}^{d_i})\right] < 1, \tag{22}$$

where $\otimes$ is the matrix Kronecker product, P is the probability transition matrix between different modes and $\rho[.]$ is the spectral radius of a matrix. □

The spectral radius result provides a necessary and sufficient condition for stability under Markovian jumps as well as a measure for the robustness of such stability. In this direction, the stability margin of the linear Markov jump system is given by $1-\rho$. In the following example, the stability margin of the observer when the observer gains are switching with a pre-specified Markovian jump policy is discussed, and it is shown how that stochastic switching policy between the observer gains provides tighter results when compared to the arbitrary switching.

Example 2: Given two high-slip and low-slip cases with the slip ratio $\lambda = \frac{R_e|\omega| - V_{xt}}{\max\{R_e|\omega|, V_{xt}\}}$ and subsequent switching actions, a probability transition matrix represents switching policies between two slip conditions. The observer gains attain either mode $\mathbf{L}_x^1 = [1.18, 387]$ or $\mathbf{L}_x^2 = [0.22, 0.1]$, corresponding to two sets of slip ratios $0 \le |\lambda| < 0.15$, $0.15 \le |\lambda|$, respectively. The probability transition matrix is in the following form:

$$\mathbf{P}_{dry} = \begin{bmatrix} 0.9 & 0.1 \\ 1-\bar{\gamma} & \bar{\gamma} \end{bmatrix}, \tag{23}$$

where $\bar{\gamma}$ is the probability that the observer stays within the high slip mode at time step $k+1$ when it is at high slip mode at time step k. The stability margin of the switched system with stochastic gain switching for different values of the angular velocity is shown in Fig. 6.

In this case, the spectral radius obtained from the arbitrary switching, which is based on the worst case gain, is 0.9960, (close to 1). It can be compared to the values plotted for stochastic switching. This substantiates that having knowledge on the policy of the switching can help us improve the stability margin (robustness) for the switched linear system. □

VI. Reliable velocity estimator in the presence of faulty measurements

Switching in observer gains is performed in order to change the level of the reliance of the observer to the force measurements. In this section, a robustness measure for velocity observers to the force measurement (estimation) failure, which acts in a cascading scheme, is proposed. Taking advantage of the newly proposed stochastic approach in the previous section, a metric (namely p_{cr}) is introduced which represents the robustness of the velocity observer to the unreliable force estimation.

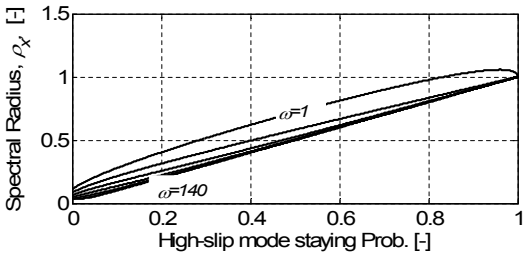

Fig. 6: Spectral radius ρ with respect to $\bar{\gamma}$.

Suppose that the measurement signal is faulty and does not reach the observer correctly with some probability p, so it can not be utilized (it is dropped) by the longitudinal/lateral observers. It is equivalent to the condition where the observer gain is $\mathbf{L}_q = \mathbf{0}$ with probability p and nonzero (active observer gain $\mathbf{L}_q$) with probability $1-p$. More formally:

$$\mathbf{e}_q[k+1] = \begin{cases} \mathbf{A}_q^d\mathbf{e}_q[k] & \text{with probability} \quad p \\ \mathbf{A}_{e_q}^d\mathbf{e}_q[k] & \text{with probability} \quad 1-p \end{cases}. \tag{24}$$

Recasting this problem into a Markovian jump analysis, one can express the probability transition matrix as:

$$\mathbf{P} = \begin{bmatrix} 1-p & p \\ 1-p & p \end{bmatrix}, \tag{25}$$

with $p_{ij} = \mathbf{Pr}(\mathcal{L}[k+1] = \mathbf{L}_q^j | \mathcal{L}[k] = \mathbf{L}_q^i)$ in which $\mathcal{L}$ is a random vector that takes values from the sample space $\mathcal{S} = \{\mathbf{L}_q, \mathbf{0}\}$. Applying Theorem 1, one can specify how tolerant the velocity observers are against faulty force measurements. This leads to the calculation of p_{cr} (namely critical probability), which is defined as the maximum allowable probability of faulty measurements occurring such that the velocity observer remains MSS.

Remark 4: In the case of measurement drop with $p < p_{cr}$, the system is no longer observable. However, since the unobservable modes are MSS, the system is stochastically detectable [42]. Figure (7) illustrates the value of the critical probability p_{cr} for different values of the wheel speed for the longitudinal and lateral velocity estimators. For probabilities larger than the p_{cr}, the system is not MSS. □

Figure (8) depicts the value of the spectral radius ρ for the longitudinal and lateral velocity estimators and different wheel speeds. This information can provide a sense of the stability margin of such systems [36].

In the following example, the stability and robustness of the system is studied in a case where the measurement signal drops with a certain probability. The values used in Example 3 are chosen to compare the conservativeness of the stability

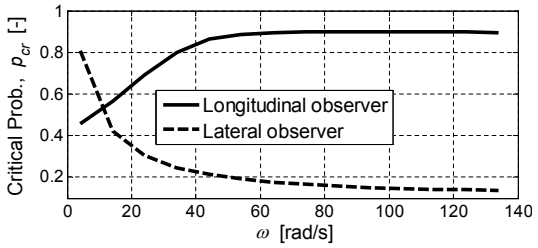

Fig. 7: Critical probabilities for the velocity observers

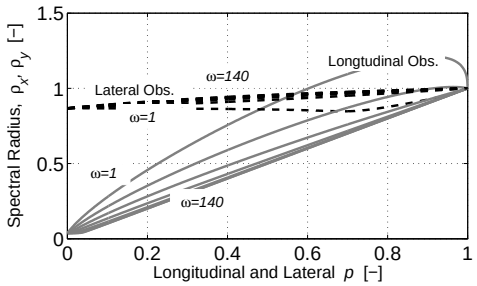

Fig. 8: Spectral radius vs. failure probability for various ω

margin of the stochastic and arbitrary switching scenarios and the value of p is not obtained from road experiment.

Example 3: Given the case where the measurement signal is dropped with $p = 0.2$ and reaches the estimator with probability $1 - p = 0.8$ (i.e. $\mathbf{L}_x = \mathbf{0}$ with $p = 0.2$ and $\mathbf{L}_x = [1.18 \quad 387]^T$ with $1-p = 0.8$), the MSS is investigated. Applying Theorem 1 in this case leads to a mean square stable system with the spectral radius $\rho = 0.9026$. Alternatively, if the measurement signal loss happens arbitrarily, based on the arbitrary switching discussed in section V, the system becomes marginally stable, i.e. $\rho = 1$. □

Therefore, investigating the faulty measurement cases with the Markovian jump model provides a less conservative criterion for the mean square stability of the estimators.

VII. Results and Discussion

This section provides results of the road experiments for the longitudinal and lateral velocity estimators on a four-wheel-independent-drive instrumented SUV with the specifications given in Table I. Different driving conditions were conducted on surfaces with different friction conditions, and the experimental results of the velocity estimators are presented and verified with the measurements from the GPS. For the road experiments, the longitudinal and lateral observer gains are $\mathbf{L}_x = [1.18 \quad 387]^T$ and $\mathbf{L}_y = [1.21 \quad 16.8]^T$, respectively. Before demonstrating the experimental results, we provide the procedure used in [29] to calculate the tire normal (vertical) force.

A. Normal force calculation

Normal forces at each corner is calculated in [29] based on lateral and longitudinal vehicle dynamics and the sprung mass angles. The longitudinal and normal acceleration components of the longitudinal dynamics are $a_{\theta x} = a_x \cos\theta_v + a_n \sin\theta_v$ and $a_{\theta n} = a_n \cos\theta_v - a_x \sin\theta_v$ where a_x, a_n are the measured longitudinal and normal accelerations by an IMU attached to the sprung mass and θ_v is the vehicle pitch angle. Normal forces at front and rear axles are calculated as

$$F_{z_f} = -\frac{m}{(d_f + d_r)}(h_{CG} a_{\theta x} - d_r a_{\theta n})$$
$$F_{z_r} = \frac{m}{(d_f + d_r)}(h_{CG} a_{\theta x} + d_f a_{\theta n}), \tag{26}$$

where the height of the vehicle's center of gravity is h_{CG}, and d_f, d_r are distances from front and rear axles to CG. Similarly, the lateral and normal acceleration components due to the lateral dynamics are $a_{\phi y} = a_y \cos\phi_v + a_n \sin\phi_v$ and $a_{\phi n} = a_n \cos\phi_v - a_y \sin\phi_v$ in which a_y is the measured lateral acceleration by IMU and ϕ_v is the vehicle roll angle. Hence, via using (26) and introducing $m_i = \frac{F_{z_i}}{g}$ where $i \in \{f, r\}$ (equivalent masses at front and rear axles), normal forces at each corner become [29]

$$F_{z_{iL}} = \frac{m_i}{T_{r_i}}\left[a_{\phi n}(\frac{T_{r_i}}{2} - h_{RC}\sin\phi_v) - a_{\phi y} h_{CG}\right]$$
$$F_{z_{iR}} = \frac{m_i}{T_{r_i}}\left[a_{\phi n}(\frac{T_{r_i}}{2} + h_{RC}\sin\phi_v) + a_{\phi y} h_{CG}\right], \tag{27}$$

where T_{r_i}, $i \in \{f, r\}$ is the length of front and rear tracks, indexes L, R denote the left and the right sides and h_{RC} is the height of the roll center. A reliable estimation of vehicle pitch and roll angles, θ_v and ϕ_v from available sensory measurements, i.e., $\dot{\theta}_v$ and $\dot{\phi}_v$, is out of the scope of this paper and we refer to [43] for more information about the procedure. The values of T_{r_f}, T_{r_r}, h_{RC}, h_{CG}, d_f and d_r which are used for the experimental tests are defined in Table I.

B. Case1: Maneuvers with longitudinal excitations

The augmented longitudinal velocity estimator with the suspension compliance is examined in a harsh launch on a surface, which has two different friction conditions and the results are shown in Fig. 9. The left wheels are on ice with $\mu \approx 0.25$, the right wheels are on a dry asphalt, and the power-train configuration is all wheel drive (AWD).

As can be seen in Fig. 9, the longitudinal estimator provides accurate velocities at each corner. The left tires are on the slippery surface at which the wheel speed $R_e\omega$ (blue lines) increases significantly due to extreme slip, while the estimated wheel center velocities at each corner (red lines) have good correspondence with the measured GPS data.

To study the effect of suspension compliance in the developed observer, Δf_n at each corner is depicted in Fig. 10 for the longitudinal estimator with and without *SC*.

Figure 10, substantiates that the incorporation of *SC* and proper observer gain allocation lead to the observed smooth and accurate velocity estimation at the CG as well as at each corner for such maneuvers with longitudinal excitations.

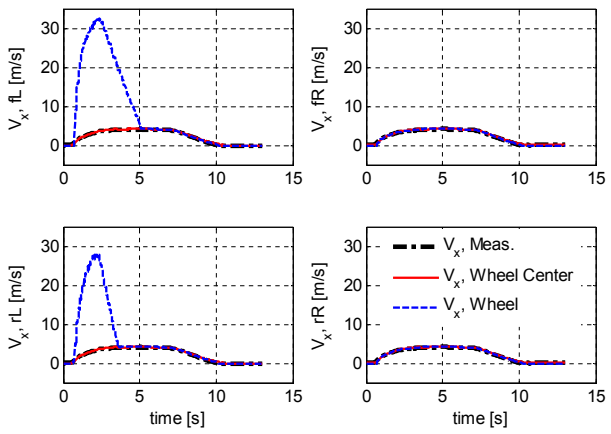

Fig. 9: Road experiments launch on split-μ (ice/dry).

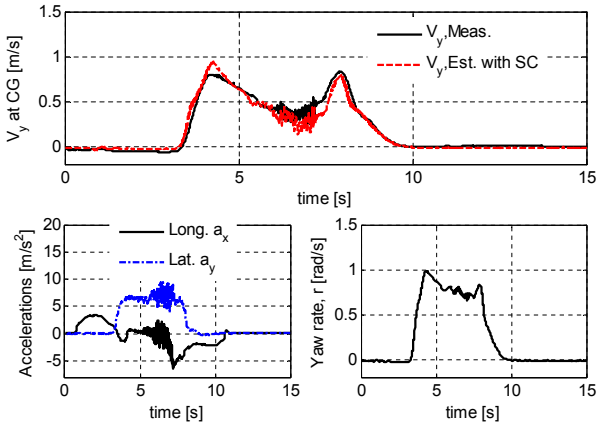

Fig. 11: Lateral velocity estimation for AiT on dry

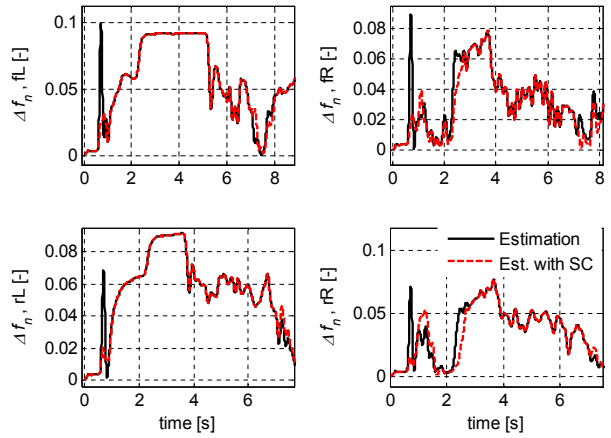

Fig. 10: Effect of the *SC* in the longitudinal forces, split-μ.

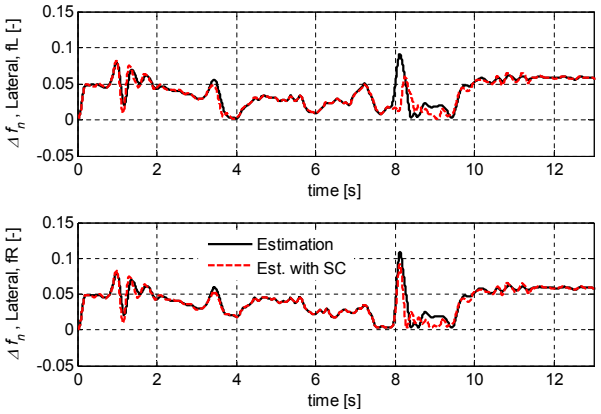

Fig. 12: Lateral force calculation errors with and without *SC*

C. Case2: Maneuvers with lateral and combined lateral/longitudinal excitations

In order to assess the corner based approach in combined-slip conditions, where the tire capacities are reduced due to a high slip ratio as well as the high slip angles in each longitudinal/lateral direction, a harsh acceleration-in-turn (AiT) maneuver with *AWD* configuration is done on a dry surface.

Results of the lateral velocity estimator together with the measured accelerations and the yaw rate are also provided in Fig. 11 for the same AiT scenario on dry asphalt.

Figure 11 reveals that high oscillations exist in both lateral and longitudinal accelerations, but the lateral state estimation methodology handles these situations and exhibits smooth and accurate outcomes. Similar to the longitudinal case, the augmented lateral estimation (by the suspension compliance) and the pure lateral observer are compared to the lateral force measurement and the difference Δf_n at the front tires are shown in Fig. 12.

Furthermore, the augmented velocity estimators are examined in the vehicle with *AWD* configuration in a harsh lane change (LC) scenario with acceleration and deceleration on snow. The experimental results of the lateral velocity estimator as well as the measured accelerations and the yaw rate are also depicted in Fig. 13 for this maneuver. Fluctuations of the measured lateral acceleration and sudden changes of the vehicle yaw rate in Fig. 13 substantiate the arduous characteristics of the driving scenario.

Normal force calculation results at each corner are also shown in Fig. 14 for this harsh LC maneuver on snow and compared with the measured vertical forces by force transducers mounted on all four wheels.

As a result, the suggested longitudinal and lateral state estimators with the suspension compliance provide good accuracy and can be used for traction and stability control systems.

VIII. Conclusion

Longitudinal and lateral vehicle's velocities with considering suspension compliance at each tire are estimated in this article. This leads to more accurate velocity estimates (slip ratio/angle) at each corner. Several road experiments with normal and harsh driving conditions have been conducted on dry and slippery

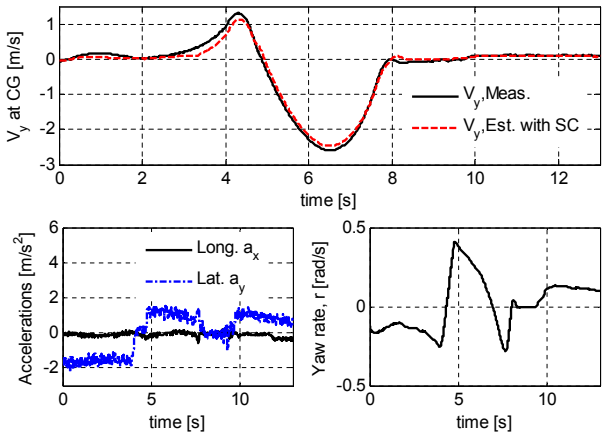

Fig. 13: Lateral velocity estimates for LC on snow

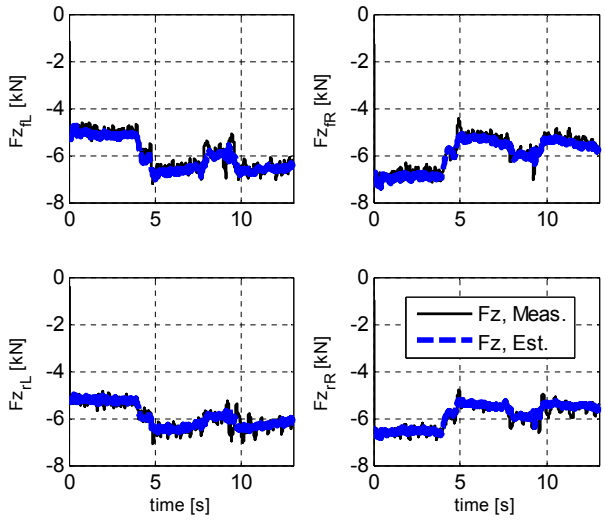

Fig. 14: Normal force estimation based on [29] at each corner

roads to validate the approach. These experiments exhibit reliable and accurate performance for a pure-slip launch, lane change maneuvers, as well as the combined-slip acceleration-in-turn scenarios. As concluded from the road experiments, the augmented estimators by *SC* can handle dry as well as slippery roads with error *RMS* less than 5.8% for the longitudinal direction and less than 7.5% for the lateral direction.

The stability of the velocity estimators are studied for the time-varying case and observer gains' arbitrary/stochastic switchings. Sensitivity of the estimators to the model parameters are also investigated for the operating regions of the varying parameter (wheel speed).

A failure in the force estimation can have a cascading effect on the velocity estimation as well. This paper presented a probabilistic measure for the resilience of the velocity estimation to such cascading failures. Deterministic and real-time analysis of such behaviour is an avenue for future studies.

ACKNOWLEDGMENT

This work was supported by Automotive Partnership Canada, Ontario Research Fund, and the General Motors Co. [grant numbers APCPJ 395996-09 and ORF-RE-04-039].

REFERENCES

[1] J. Ryu and J. C. Gerdes, "Integrating inertial sensors with global positioning system (GPS) for vehicle dynamics control," *Journal of Dynamic Systems, Measurement, and Control*, vol. 126, no. 2, pp. 243–254, 2004.

[2] L. Imsland, T. A. Johansen, T. I. Fossen, H. F. Grip, J. C. Kalkkuhl, and A. Suissa, "Vehicle velocity estimation using nonlinear observers," *Automatica*, vol. 42, no. 12, pp. 2091–2103, 2006.

[3] L. H. Zhao, Z. Y. Liu, and H. Chen, "Design of a nonlinear observer for vehicle velocity estimation and experiments," *IEEE Transactions on Control Systems Technology*, vol. 19, no. 3, pp. 664 – 672, 2011.

[4] L. Imsland, H. F. Grip, T. A. Johansen, T. I. Fossen, J. C. Kalkkuhl, and A. Suissa, "Nonlinear observer for vehicle velocity with friction and road bank angle adaptation-validation and comparison with an extended kalman filter," SAE Technical Paper, Tech. Rep., 2007.

[5] H. Guo, H. Chen, F. Xu, F. Wang, and G. Lu, "Implementation of ekf for vehicle velocities estimation on fpga," *IEEE Transactions on Industrial Electronics*, vol. 60, pp. 3823–3835, 2013.

[6] T. a. Wenzel, K. J. Burnham, M. V. Blundell, and R. a. Williams, "Dual Extended Kalman Filter for Vehicle State and Parameter Estimation," *Vehicle System Dynamics*, vol. 44, no. 2, pp. 153–171, 2006.

[7] G. Baffet, A. Charara, and G. Dherbomez, "An observer of tire–road forces and friction for active security vehicle systems," *Mechatronics, IEEE/ASME Transactions on*, vol. 12, no. 6, pp. 651–661, 2007.

[8] X. Huang and J. Wang, "Robust Sideslip Angle Estimation for Lightweight Vehicles Using Smooth Variable Structure Filter," *ASME Dynamic Systems and Control Conference*, pp. 1–8, 2013.

[9] M. Wielitzka, M. Dagen, and T. Ortmaier, "State estimation of vehicle's lateral dynamics using unscented kalman filter," *Decision and Control (CDC), 2014 IEEE 53rd Annual Conference on*, pp. 5015–5020, 2014.

[10] C. C. D. Wit, H. Olsson, K. J. Astrom, and P. Lischinsky, "A New Model for Control of Systems with Friction," *IEEE TRANSACTIONS ON AUTOMATIC CONTROL*, vol. 40, 1995.

[11] C. C. D. Wit and P. Tsiotras, "Dynamic Tire Friction Models for Vehicle Traction Control," *Proceedings of the 38th Conference on Decision and Control*, 1999.

[12] M. Canale, L. Fagiano, and C. Novara, "A dvs-mhe approach to vehicle side-slip angle estimation," *Control Systems Technology, IEEE Transactions on*, vol. 22, no. 5, pp. 2048–2055, 2014.

[13] M. Tanelli, A. Ferrara, and P. Giani, "Combined vehicle velocity and tire-road friction estimation via sliding mode observers," *IEEE International Conference on Control Applications*, 2012.

[14] H. Faer Grip, L. Imsland, T. A. Johansen, J. C. Kalkkuhl, and A. Suissa, "Vehicle sideslip estimation: Design, implementation, and experimental validation," *IEEE control systems*, vol. 29, no. 5, pp. 36–52, 2009.

[15] X. Zhang, Y. Xu, M. Pan, and F. Ren, "A vehicle ABS adaptive sliding-mode control algorithm based on the vehicle velocity estimation and tyre/road friction coefficient estimations," *Vehicle System Dynamics*, vol. 52, no. 4, pp. 475–503, 2014.

[16] C. Ahn, H. Peng, and H. E. Tseng, "Robust estimation of road frictional coefficient," *Control Systems Technology, IEEE Transactions on*, vol. 21, no. 1, pp. 1–13, 2013.

[17] Y. Chen and J. Wang, "Adaptive vehicle speed control with input injections for longitudinal motion independent road frictional condition estimation," *IEEE Transactions on Vehicular Technology*, vol. 60, pp. 839–848, 2011.

[18] E. Hashemi, A. Kasaiezadeh, S. Khosravani, A. Khajepour, N. Moshchuk, and S. K. Chen, "Estimation of longitudinal speed robust to road conditions for ground vehicles," *Vehicle System Dynamics*, vol. 54, pp. 1120–1146, 2016.

[19] C. Canudas-de Wit, P. Tsiotras, E. Velenis, M. B. Gissinger, and G. Gissinger, "Dynamic Friction Models for Road/Tire Longitudinal Interaction," *Vehicle System Dynamics*, vol. 39, pp. 189–226, 2003.

[20] E. Hashemi, M. Pirani, A. Khajepour, and A. Kasaiezadeh, "A comprehensive study on the stability analysis of vehicle dynamics with pure/combined-slip tyre models," *Vehicle system dynamics*, vol. 54, no. 12, pp. 1736–1761, 2016.

[21] R. Tóth, *Modeling and identification of linear parameter-varying systems*. Springer, Berlin, 2010, vol. 403.

[22] G. Baffet, A. Charara, and D. Lechner, "Estimation of vehicle sideslip, tire force and wheel cornering stiffness," *Control Engineering Practice*, vol. 17, no. 11, pp. 1255–1264, 2009.

[23] R. Rajamani, G. Phanomchoeng, D. Piyabongkarn, and J. Y. Lew, "Algorithms for real-time estimation of individual wheel tire-road friction coefficients," *Mechatronics, IEEE/ASME Transactions on*, vol. 17, no. 6, pp. 1183–1195, 2012.

[24] S. Mammar, S. Glaser, and M. Netto, "Vehicle lateral dynamics estimation using unknown input proportional-integral observers," *American Control Conference*, pp. 6–12, 2006.

[25] Y. Wang, D. M. Bevly, and S.-k. Chen, "Lateral tire force estimation with unknown input observer," *ASME 2012 5th Annual Dynamic Systems and Control Conference joint with the JSME 2012 11th Motion and Vibration Conference*, pp. 531–538, 2012.

[26] M. Doumiati, A. Victorino, D. Lechner, G. Baffet, and A. Charara, "Observers for vehicle tyre/road forces estimation: experimental validation," *Vehicle System Dynamics*, vol. 48, no. 11, pp. 1345–1378, 2010.

[27] W. Cho, J. Yoon, S. Yim, B. Koo, and K. Yi, "Estimation of tire forces for application to vehicle stability control," *Vehicular Technology, IEEE Transactions on*, vol. 59, no. 2, pp. 638–649, 2010.

[28] E. Hashemi, A. Kasaeizadeh, A. Khajepour, N. Mushchuk, and S.-K. Chen, "Robust Estimation and Experimental Evaluation of Longitudinal Friction Forces in Ground Vehicles," in *ASME IMECE2014*, 2014.

[29] E. Hashemi, M. Pirani, A. Khajepour, B. Fidan, A. Kasaiezadeh, S. Chen, and B. Litkouhi, "Integrated estimation structure for the tire friction forces in ground vehicles," in *Advanced Intelligent Mechatronics, 2016 IEEE Conference on*. IEEE, 2016.

[30] J. E. Slotine and W. Li, "Applied nonlinear control," *Prentice hall*, 1991.

[31] A. Czornik, A. Nawrat, M. Niezabitowski, and A. Szyda, "On the lyapunov and bohl exponent of time-varying discrete linear system," *20th Mediterranean Conference on Control & Automation (MED)*, pp. 194–197, 2012.

[32] T. Berger, "Bohl exponent for time-varying linear differential-algebraic equations," *Int. J. Control*, vol. 85, pp. 1433–1451, 2012.

[33] H. Khalil, *Nonlinear systems*. Prentice hall, 1996.

[34] H. Lin and P. J. Antsaklis, "Stability and stabilizability of switched linear systems: a survey of recent results," *Automatic control, IEEE Transactions on*, vol. 54, no. 2, pp. 308–322, 2009.

[35] D. Liberzon, *Switching in systems and control*. Boston, MA, USA: Birkhuser, 2003.

[36] O. L. V. Costa, M. D. Fragoso, and R. P. Marques, "Discrete-time markov jump linear systems," *Springer, London*, 2006.

[37] T. B. Hoang, W. P. Lepine, A. D. Bernardinis, and M. Netto, "Extended braking stiffness estimation based on a switched observer, with an application to wheel-acceleration control," *IEEE Transactions on Control Systems Technology*, vol. 22, no. 6, pp. 2384 – 2392, 2014.

[38] L. Zhang and E. Boukas, "Stability and stabilization of markovian jump linear systems with partly unknown transition probabilities," *Automatica*, vol. 45, pp. 463–468, 2009.

[39] O. L. V. Costa, M. D. Fragoso, and R. P. Marques, "Continuous time markovian jump linear systems," *Springer, Berlin*, 2005.

[40] P. Seiler and R. Sengupta, "Analysis of communication losses in vehicle control problems," *In Proceedings of the 2001 American Control Conference*, pp. 1491–1496, 2001.

[41] V. Gupta, R. M. Murray, L. Shi, and B. Sinopoli, *Network sensing, estimation and control systems*. Dept. Control Dyn. Syst., California Inst. Technol., Pasadena, CA, USA, Tech. Rep., 2009.

[42] V. Dragan and T. Morozan, "Observability and detectability of a class of discrete-time stochastic linear systems," *IMA Journal of Mathematical Control and Information*, vol. 23, pp. 371–394, 2006.

[43] H. Guo, H. Chen, F. Xu, F. Wang, and G. Lu, "Estimation of vehicle roll angle," *International Symposium on Communications, Control and Signal Processing*, pp. 1–4, 2010.

Mohammad Pirani received the BSc degree in mechanical engineering from Amirkabir University of Technology (Tehran Polytechnic) in 2011 and MASc degree in electrical and computer engineering from the University of Waterloo, Waterloo, ON, Canada, in 2014. He is currently working toward the PhD degree in the Department of Mechanical and Mechatronics Engineering, University of Waterloo. His research interests include resilient and fault tolerant control, networked control systems, and multi-agent systems.

Ehsan Hashemi is currently working toward the PhD degree in the Department of Mechanical and Mechatronics Engineering, University of Waterloo, Waterloo, ON, Canada. He received his M.Sc. in Mechanical Engineering from Amirkabir University of Technology (Tehran Polytechnic), Tehran, Iran. His previous work includes biped locomotion, control and state estimation of mobile robots, and multibody dynamics. His research interests are distributed and fault-tolerant estimation, robust control, vehicle active safety systems, and dynamical systems.

Amir Khajepour is a Professor of mechanical and mechatronics engineering with the University of Waterloo, Waterloo, ON, Canada, and the Canada Research Chair in Mechatronic Vehicle Systems. He has developed an extensive research program that applies his expertise in several key multidisciplinary areas. His research interests include system modeling and control of dynamic systems. His research has resulted in several patents and technology transfers. He is the author of more than 350 journal and conference publications and five books. He is a Fellow of the Engineering Institute of Canada, the American Society of Mechanical Engineers, and the Canadian Society of Mechanical Engineering.

Baris Fidan "(S'02 – M'04 – SM'11)" received the B.S. degrees in electrical engineering and mathematics from Middle East Technical University Turkey in 1996, the M.S. degree in electrical engineering from Bilkent University, Turkey in 1998, and the Ph.D. degree in electrical engineering at the University of Southern California, USA in 2003. He is currently an associate professor in the Mechanical and Mechatronics Engineering Department, University of Waterloo, Canada. His research interests include cooperative and adaptive control with vehicular applications, system identification, sensor networks, and nonlinear systems.

Alireza Kasaiezadeh received the B.Sc. and M.Sc. degrees from Sharif University of Technology, Tehran, Iran, and the Ph.D. degree in mechanical and mechatronic engineering from the University of Waterloo, Waterloo, ON, Canada. He did a two-year postdoctoral fellowship and was a Research Assistant Professor with the University of Waterloo. He is currently a Senior Researcher with GM Technical Center, General Motors Company, Warren, MI, USA, where he is working in the area of automated driving and vehicle control. He has more than 14 years of industrial experience in the automotive industry and, in particular, in active safety systems, chassis control system design, and field testing. His research interests include automated driving, vehicle dynamics, control and optimization.

Shih-Ken Chen received the B.S. degree from National Taiwan University, Taipei, Taiwan, in 1985; the M.S. degree in mechanical engineering from the University of WisconsinMadison, Madison, WI, USA, in 1990; and the Ph.D. degree in mechanical engineering from Massachusetts Institute of Technology, Cambridge, MA, USA, in 1996. He then joined the Research and Development Center, General Motors Corporation. He is currently a Staff Researcher with the GM Technical Center, General Motors Company, Warren, MI, USA. His previous work includes collision avoidance systems, electronic stability control, active all-wheel-steer control, and rollover avoidance. His current research interests include holistic chassis and vehicle control for both conventional driveline and electric driveline, driver-in-the-loop vehicle control, and vehicle active safety system and automated driving.

Bakhtiar Litkouhi received the B.Sc. degree in mechanical engineering from Arya-Mehr (Sharif) University of Technology, Iran and the M.Sc. degree in applied mathematics and the Ph.D. degree in systems science, specializing in control, both from Michigan State University, East Lansing, MI, USA. He was an Assistant Professor with Oakland University, Rochester, MI, USA. He has served as the Program Manager for several large-scale projects in automated and intelligent vehicle systems, human machine interface, and integrated vehicle control, where he has made many contributions through numerous patents, publications, and presentations. He is currently the Manager of Automated Driving and Vehicle Control Systems, General Motors Global Research and Development, Warren, MI, USA. In addition to his current responsibilities, he is a board member of the Intelligent Transportation Society of Michigan, a member of the Board of Directors of the Waterloo Center for Automotive Research (WatCAR), and the Program Manager of GMCarnegie Mellon University Autonomous Driving Collaborative Research Lab.